The polySTRAND model of flow-induced nucleation in polymers

Daniel J. Read[1], Claire McIlroy[2,3], Chinmay Das[1], Oliver G. Harlen[1], and Richard S. Graham[3]
[1]*School of Mathematics, University of Leeds, Leeds LS2 9JT, UK.*
[2]*School of Mathematics and Physics, University of Lincoln, Lincoln, LN6 7TS, UK.*
[3]*School of Mathematical Sciences, University of Nottingham, Nottingham NG7 2RD, UK.*
(Dated: February 14, 2020)

We develop a thermodynamic continuum-level model, polySTRAND, for flow-induced nucleation in polymers suitable for use in computational process modelling. The model's molecular origins ensure it accounts properly for flow and nucleation dynamics of polydisperse systems and can be extended to include effects of exhaustion of highly deformed chains and nucleus roughness. It captures variations with the key processing parameters, flow rate, temperature and molecular weight distribution. Under strong flow, long chains are over-represented within the nucleus, leading to super-exponential nucleation rate growth with shear rate as seen in experiments.

PACS numbers: 64.70.km, 64.60.qe, 83.80.Sg

Crystal nucleation in polymers is strongly enhanced by flow [1, 2], and this flow-induced crystallisation (FIC) is a prominent unsolved problem in polymer physics. FIC is an externally driven, non-equilibrium phase transition that controls crystallisation in industrial polymer processing. Hence, a molecular understanding of FIC would enable design of semi-crystalline products by tailoring processing conditions. This requires a quantitative model for the key control parameters of temperature, flow rate and molecular weight distribution (MWD).

Flow rapidly accelerates the crystallisation kinetics through an enhanced nucleation rate, $\dot{N}$ (see Fig.1). Beyond this, even stronger flow produces the aligned shish kebab morphology [2–4]. Both nucleation and alignment increase with flow rate, strain, molecular weight and long chain concentration [3–12]. Despite substantial experimental progress, key obstacles remain [13]: (1) nucleation events are rare, rapid and spatially localised, so experiments make observations long after critical nucleation has occurred; (2) synthesising monodisperse crystallizable polymers is difficult so most FIC experiments involve broad MWDs. Under flow, such melts have a wide range of chain deformation, and nucleation results from the cooperation of many chains of widely differing deformation and concentration. Polydispersity is ubiquitous in experiments and processing, but obscures the central physics of flow-induced nucleation (FIN).

Molecular dynamics (MD) simulations can complement experiments. Recent simulations have resolved individual nucleation events from monodisperse chains, to quantify FIN [14–19]. Simulations of 150-carbon polyethylene [15], showed that the Kuhn segment nematic order, $P_{2,K}$, is the key parameter for FIN. However, MD simulations cannot reach the MWD and undercooling required to directly model experiments or industrial processing. At much higher coarse-graining, continuum models comprise deterministic differential equations [20–24]. These can access long spatiotemporal scales but currently struggle with polydispersity: they use insufficiently detailed rheological models and do not account for nucleation from multiple chains with different deformations. At intermediate coarse-graining is the GO model [25, 26], which simulates the nucleation dynamics stochastically but uses a constitutive equation for the amorphous chain dynamics. It can access long chains and low-undercooling. Despite encouraging comparisons with experiments [25, 27], the model lacks a constitutive equation valid for polydisperse melts [25] and is too expensive for computational modelling of polymer processing [13].

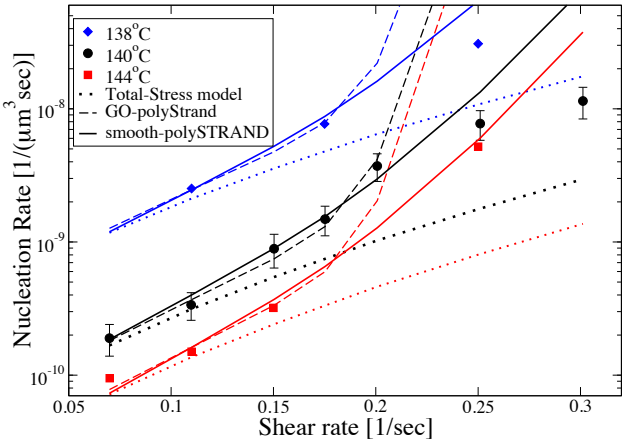

FIG. 1. Steady-state $\dot{N}$ measurements against $\dot{\gamma}$ for an iPP melt[9] and the polySTRAND model predictions. The total-stress model pre-averages chain deformation into a single species.

We present a comprehensive resolution to the above long-standing issues by uniting multiple levels of coarse-graining, including MD, kinetic Monte Carlo and continuum modelling, to produce a computationally fast analytic model with deep molecular roots: we recalibrate the GO model to recent MD simulations [15]; we use a recent constitutive equation [28] for polydisperse melts; and we derive a novel analytic solution of the GO model [25, 26]. This leads to a fully polydisperse model of FIN

- the POLYdisperse STRain Accelerated Nucleation Dynamics (polySTRAND) model. We derive two sub models: GO-polySTRAND closely captures the GO model; smooth-polySTRAND captures experiments by including a nucleus roughness penalty and local exhaustion of long chains. Fig.1 summarises our main results, to be discussed in more detail below: (i) a simple average across the polymer chain population (total-stress model), which does not properly account for the effects of polydispersity, is insufficient to predict the strong acceleration of nucleation rate with $\dot{\gamma}$; (ii) polydispersity leads to enrichment of long chains in the critical nucleus, giving a super-exponential dependence of the nucleation rate on shear (GO-polySTRAND); and (iii) this enrichment is limited: local exhaustion of long chains (smooth-polySTRAND) limits this super-exponential behaviour.

Model overview: In the GO model nuclei are ellipsoids of N_S stems and N_T monomers (Fig 2a). The quiescent nucleus potential is $U_{\rm nuc} = -\epsilon_B N_T + \mu_S S(N_T, N_S)$, where ϵ_B is the free energy of crystallization per monomer, μ_S is the surface energy cost, and S is the surface area. All energies are in units of k_BT. The model assumes that the flow-induced reduction in chain entropy can be subtracted from the entropy penalty for crystallization. Each chain species deforms differently so has its own attachment rate. The stem attachment k_{st}^+ and detachment k_{st}^- rates obey $k_{st}^+/k_{st}^- = \phi_i \exp(-\Delta U_{\rm nuc} + \Delta f_i)$, where ϕ_i is the melt volume fraction of species i and Δf_i is the change in monomer free energy from chain deformation. Existing stems can attach or detach a monomer of the same species whose volume fraction at the nucleus surface taken as 1. Thus the ratio of rates for existing stems is identical to k_{st}^+/k_{st}^- but with $\phi_i = 1$.

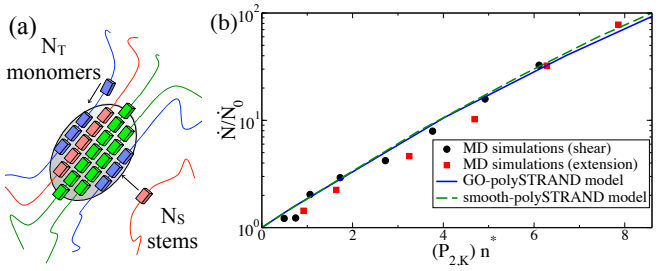

FIG. 2. (a) A nucleus in the GO model [25]. Blocks are crystallised segments, smooth lines are amorphous. Colours are chains with different deformation. Each chain forms a separate stem. (b) Nucleation rate over quiescent rate against Kuhn step nematic order for MD [15] and the our models. The quiescent critical nucleus, n^*, in MD is 12 Kuhn steps.

GO-polySTRAND: We derive an analytical expression for the nucleus free energy consistent with the GO model. The nucleus has stems of species i with fraction w_i (number of i stems is $N_S w_i$) and monomers with fraction v_i (number of i monomers is $N_T v_i$). The nucleus entropy contains (i) the number of arrangements of $N_S w_i$ stems of each species among N_S stems, and (ii) the number of ways to distribute $N_T v_i$ monomers among $N_S w_i$ stems. For $q = N_S/N_T$ and large N_S and N_T the nucleus free energy is (see Supplementary Information (SI) [29] §1):

$$\begin{aligned} F = N_T \sum_i \big[& q w_i (2 \log w_i - \log \phi_i) - v_i \log v_i \\ & + (v_i - q w_i) \log (v_i - q w_i) - v_i \Delta f_i \big] \\ & + N_S \log q - \epsilon_B N_T + \mu_S S(N_T, N_S), \end{aligned} \tag{1}$$

Minimisation over $\{w_i, v_i\}$ with $\sum_i w_i = \sum_i v_i = 1$ yields

$$w_i = \frac{B \phi_i \exp(\Delta f_i)}{1 - A \exp(\Delta f_i)}, \; v_i = \frac{B q \phi_i \exp(\Delta f_i)}{[1 - A \exp(\Delta f_i)]^2}, \tag{2}$$

where A and B are Lagrange multipliers, determined by,

$$\sum_i \frac{q \phi_i \exp(\Delta f_i)}{(1 - A \exp(\Delta f_i))^2} = \sum_i \frac{\phi_i \exp(\Delta f_i)}{1 - A \exp(\Delta f_i)}; \;\; B = \frac{1}{\sum_i \frac{\phi_i \exp(\Delta f_i)}{1 - A \exp(\Delta f_i)}}$$

Here, the first equation is solved numerically for A (there is always a suitable A such that the denominators are positive) and the second gives B directly. The GO-polySTRAND is computationally fast, only requiring numerical solution of the equation for A. The model also enables addition of further physics without costly microscopic simulations.

Eq.1 is projected onto N_T alone by minimising over N_S and approximating fluctuations in N_S via $\partial^2 F / \partial N_S^2$ (see SI [29] §1.3). The same algorithm computes the quiescent free energy, leading to the change in free energy $\Delta F_{\rm pS} = F_{\rm pS}^{\rm q} - F_{\rm pS}^{\rm flow}$, cancelling some of the error from finite N_S. The exact calculation of the quiescent barrier from ref [27] provides the final free energy barrier via $F_{\rm final} = F_{\rm GO}^{\rm q} - \Delta F_{\rm pS}$. Barriers from this method agree very closely with GO simulations [27] (see SI [29] §1.4). We calculate $\dot{N}$ by solving a 1D Kramer's problem [30], which accurately predicts $\dot{N}$ from GO simulations for a given nucleation barrier [27] (see SI [29] §3).

Next, we require $\{\Delta f_i\}$. In MD simulations [15] of two-entanglement chains, $\dot{N}$ grows exponentially with the Kuhn segment nematic order $P_{2,K}$. Here, head-to-tail symmetry means there is effectively one species. For a single species at moderate Δf_i, polySTRAND predicts $\dot{N} \propto \exp(\Delta f n^*)$, where n^* is the quiescent critical nucleus size. Hence taking $\Delta f = \Gamma P_{2,K}$, with Γ a constant, gives the exponential behaviour seen in MD and $\Gamma = 0.65$ gives quantitative agreement (Fig 2b). A polydisperse melt requires $P_{2,K}$ for each chain length. Hence we use the Rolie-Double-Poly (RDP) constitutive equation [28] to compute chain configuration tensors $\mathbf{A}$ under flow for each species. The MWD is discretized into N species, with species i having fraction ϕ_i and Z_i entanglements. The RDP computes $\mathbf{A}_{ij}$, the effect of species j on species i, via N^2 coupled differential equations. The overall configuration for species i is $\mathbf{A}_i = \sum_j \phi_j \mathbf{A}_{ij}$. The order parameter for species i is $P_{2,K,i} = \Lambda_{\rm max}/N_e$, where $\Lambda_{\rm max}$ is

the largest eigenvalue of $\mathbf{A}_i - \mathbf{I}$ and N_e is the Kuhn steps per entanglement. The RDP enables us to resolve $P_{2,K}$ for each chain length and then use the polySTRAND model to compute their co-operative effect on nucleation. We also compare this to a simplified 'total-stress' model where the total melt stress ($\mathbf{A}_T = \sum_i \phi_i \mathbf{A}_i$) is used to compute a pre-averaged single species $P_{2,K,av}$.

Fig 1 shows steady-shear $\dot{N}$ measurements from a polydisperse isotactic polypropylene (iPP) [9]. The total-stress model predicts $\dot{N}$ is, at most, exponential in the shear rate, $\dot{\gamma}$, since $P_{2,K,av}$ grows sublinearly with $\dot{\gamma}$ for a shear thinning fluid. In contrast, the GO-polySTRAND captures the upward curvature in the data at all temperatures. This arises directly from enrichment of highly-deformed chains in the nucleus (Eq 2 indicates strong enrichment in the fraction w_i of stems with large Δf_i, i.e. oriented chains, predisposed to nucleation, and further enrichment in v_i); this long-chain enrichment, as well as a flow model capable of predicting individual chain species dynamics, is indispensable to model $\dot{N}$.

Long-chain enrichment apparently contradicts scattering data by Kimata *et al.* [3], showing no overrepresentation of long chains in shish structures. However, our model predicts enrichment only in pre-critical nuclei. Post-nucleation growth is thermodynamically favourable so recruits all chains equally, giving the melt distribution in well-developed crystals. Thus enrichment strongly influences $\dot{N}$, but will not be observed in larger crystals. Indeed Kimata *et al.* observed that the long chains catalyse the recruitment of other chains into shish. To quantitatively understand shish formation, we require a detailed understanding of polydispersity in point-like nucleation, as provided by the polySTRAND model.

The model parameters required for experimental comparison fall into four classes: (i) material (Kuhn step density ρ_K and crystal growth rate G_c) and (ii) rheological parameters (entanglement molecular weight M_e, Rouse time of an entanglement segment τ_e and N_e): these are obtained from the literature or linear rheological measurements; (iii) quiescent nucleation parameters (monomer attachment time τ_0, and the quiescent nucleation barrier, specified by n^* and the quiescent barrier height ΔF_q^*, or equivalently μ_S and ϵ_B) which are obtained from the quiescent crystallisation measurements; and (iv) a single, order 1, FIC parameter (Γ), which is fitted to low-shear FIC experiments (see SI [29] §4). All parameters are independent of MWD, except for τ_e which depends weakly on MWD. Only certain parameters (τ_e, n^* and ΔF_q^*) depend on temperature. To model the data in Fig.1 at 140°C, we took the material and rheological parameters from ref [25]: $M_e = 4.4$kg mol^{-1}, $\tau_e = 90$ns, $N_e = 25$, $\rho_K = 2.7 \times 10^9 \mu$m^{-3}, $\tau_0 = 0.76$ns and $n^* = 1000$ monomers (G_c is not required to model the nucleation rate). We modeled the MWD as a generalized exponential distribution, as implemented in the RepTate software [31] with parameters selected to give the reported M_w and M_n. We adjusted the quiescent barrier height ΔF_q^* and Γ to capture the lowest two shear rates at 140°C, obtaining $65.0 k_B T$ and 4.3, respectively. Finally, we slightly enhanced the high-molecular weight tail to capture the curvature of the 140°C experiments, adding a mode of mass 1.9×10^5 kg mol^{-1} at $\phi = 0.03\%$. To model the other temperatures we adjusted *only* ϵ_B to capture the lowest $\dot{\gamma}$, obtaining ΔF_q^* of 63.8 and $66.7 k_B T$ at 130, and 144°C, respectively.

Smooth-polySTRAND: The GO-polySTRAND overpredicts the curvature at high $\dot{\gamma}$ (Fig.1) suggesting a bound to the enrichment of deformed chains. This may be because nucleus growth allows insufficient time to draw stems from an infinite supply in the surrounding melt. Instead stems are drawn from a small region around the nucleus. Also, the GO-polySTRAND model allows the nucleus to be composed of stems of widely different lengths: this is unfavourable, as only stems of similar length benefit fully from crystallization. We account for these as follows. (1) A growing nucleus draws N_S stems at fraction w_i, from a *limited* number Q_S of stems with initial fraction $\{\phi_i\}$, leaving $Q_S - N_S$ remaining stems at fraction θ_i, such that $(Q_S - N_S)\theta_i + N_S w_i = Q_S \phi_i$. We replace the term $-N_S \sum_i w_i \log \phi_i$ in Eq. 1 with $\sum_i [(Q_S - N_S)\theta_i \log \theta_i - Q_S \phi_i \log \phi_i]$, the change in stem translation entropy between the initial melt (Q_s stems at fraction ϕ_i) and the final depleted melt ($Q_s - N_s$ stems at fraction θ_i). (2) We penalise deviations of the stem length l (in monomers) from the average $L = N_T/N_S$, via an energy $\frac{1}{2}\kappa(l-L)^2$. We now proceed as with the GO-polySTRAND model by deriving the nucleus free energy. A partition sum over stem lengths at fixed N_T gives this to be (see SI [29] §2):

$$
\begin{aligned}
F = &\sum_i [(Q_S - N_S)\theta_i \log \theta_i - Q_S \phi_i \log \phi_i + N_S w_i \log w_i] \\
&- N_T \mathrm{E}(\Delta f) - (N_S/2\kappa)\mathrm{Var}(\Delta f) + \tfrac{1}{2} \log N_S \\
&- \tfrac{1}{2}(N_S - 1)\log(2\pi/\kappa) - \epsilon_B N_T \ + \mu_S S(N_T, N_S)
\end{aligned}
$$

where $\mathrm{E}(\Delta f)$ and $\mathrm{Var}(\Delta f)$ are the mean and variance of Δf_i over distribution w_i. Minimisation over $\{w_i\}$ gives the chemical equilibrium of stems between the nucleus and the locally surrounding melt:

$$
w_i = \frac{Q_S \phi_i}{N_S + B(Q_S - N_S)\exp((P/\kappa - L)\Delta f_i - \Delta f_i^2/2\kappa)},
$$

where B and P are determined from $\sum_i w_i = 1$ and $\sum_i w_i \Delta f_i = P$. We use $Q_S = Q_{S0} N_S$, so the number of available stems grows with N_S, and $\kappa = \kappa_0 + 1/L^2$, so κ is sufficiently large for all relevant nucleus shapes. This adds two FIC parameters, Q_{S0} and κ_0, which are fitted to experiments in Fig 1. The final barrier is computed directly, as we have no exact solution to the quiescent problem as in GO-polySTRAND, and the nucleation rate is calculated as before (see SI [29] §3). Fig. 1 shows improved agreement at high $\dot{\gamma}$ due to local exhaustion of

long chains; here we fitted $Q_{S0} = 30$ and $\kappa_0 = 0.1$. To capture the data, we also needed to slightly increase the mass of the extra high-molecular weight mode to 3.0×10^5 kg mol^{-1}.

We verify the model for varying MWD using the experiments of Acierno *et al.* [32], who studied a range of isotactic poly-1-butene (iPB) melts (see Fig 3). These FIC experiments applied a constant $\dot\gamma$ for time t_s, so that $\dot\gamma t_s = 60$, and recorded the half-time of the resulting turbidity evolution, $t_{1/2}$, all at 103°C. In all cases $t_s \ll t_{1/2}$. Such measurements are invariably affected by heterogeneous nucleation due to embedded particles that provide a favourable surface for nucleation [18, 19]. To model these data we assume: the heterogeneous nucleation density, N_0, at 103°C, varies by sample; quiescent homogeneous nucleation and post-shear nucleation are negligible; shear creates $\dot N_{\dot\gamma} t_s$ extra nuclei, where $\dot N_{\dot\gamma}$ is the steady-state FIN rate from the smooth-polySTRAND model; the FIN barrier at zero shear (characterized by ΔF_q^* and n^*) and all other crystallisation parameters do not vary between samples; and $t_{1/2}$ occurs when the crystal fraction reaches $\phi_c = 10\%$, although our conclusions are insensitive to the exact value. Thus we computed $t_{1/2}$ by combining $\dot N_{\dot\gamma} t_s$ and N_0 in the Schneider rate equations [33]. We obtained model parameters as follows. Rheological parameters were fitted to linear rheological measurements (see SI [29] §4.3). The growth rate for iPB at 103°C [34] is $G = 0.063\mu$m/sec. We computed $\rho_K = 5.3\times10^8\mu$m^{-3} from the melt density and $\tau_0 = 0.31\mu$s by projecting τ_e to the Kuhn step length-scale. The quiescent $t_{1/2}$ determines N_0, giving values of $1.3, 8.3, 12$ and $37\times10^{-12}\mu$m^{-3}, respectively, for iPB116, 177, 295 and 398. We took $Q_{S0} = 30$ and $\kappa_0 = 0.1$ from our iPP modelling above. We fitted the remaining parameters, Γ and ΔF_q^* and n^*, to the FIC data for iPB166 *only*, giving 1.3, $68k_BT$ and 540, respectively. In summary, all samples required fitting to linear rheology and quiescent crystallisation data, while a single FIC parameter Γ was fitted to FIC data for the lowest molecular weight *only*. Fig 3 shows the model predicts $t_{1/2}$, for all samples, whenever there are isotropic crystals, up to the emergence of rod-like crystals, successfully predicting the effect of varying MWD. Where there are entirely rod-like crystals the model generally predicts a lower $t_{1/2}$ than experiments. This could be due to overprediction of $\dot N$ at high $\dot\gamma$, as in Fig 1. Also absent from our model is the slower crystallisation kinetics of rod-like crystals, compared to spherulites, due to their lower growth dimension. The model overpredicts $t_{1/2}$ for the highest M_w at the lowest $\dot\gamma$. Here, the nucleation density is very high and t_s is long, suggesting that crystallisation during the flow may be non-negligible.

Conclusions: Using systematic multiscale modelling we derived a highly tractable model of FIN with deep-rooted molecular origins. We used MD [15] as a high-resolution pseudo-experiment to extract the key physics of FIN; we extended the spatiotemporal range with highly coarse-grained kinetic Monte Carlo simulations [25, 26]; and, via a low-dimensional projection and thermodynamic modelling, we produced a rapidly solvable model for FIN. Our coordination of these techniques provides a road-map for problems with very widely separated spatiotemporal scales, common throughout molecular physics. Our thermodynamic modelling provides a flexible, analytic and broadly-applicable framework to capture general anisotropic nucleation under external fields. We illustrated this flexibility by adding local exhaustion of long chains and a penalty for nucleus roughness. Future extensions of this approach may produce a fully non-equilibrium treatment of diffusion and concentration gradients around the nucleus. Using a recent nonlinear flow model, we account properly for the dynamics of each chain species, not just the total stress. Our FIN model makes successful quantitative predictions for variations with flow rate, temperature and molecular weight distribution, which are key processing control parameters. Our model predicts the enrichment of long chains during nucleation. A signature of this enrichment, seen in experiments, is super-exponential growth of $\dot N$ with $\dot\gamma$. This super-exponential effect vanishes in single species models. Our FIN model is nearly analytic, so is suitable for computational modelling of polymer processing. The models in this letter are available in the Reptate software [31]

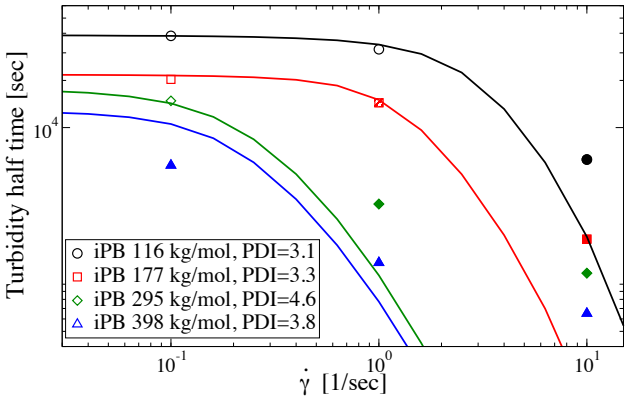

FIG. 3. Experiments [32] and the smooth-polySTRAND for $t_{1/2}$ after a shear of $\gamma = 60$ for iPB. The legend shows M_w and M_w/M_n (PDI). The open, closed and shaded symbols indicate spherical, rod and mixed morphologies, respectively.

We thank Victor Boudara for useful discussions and Quan Chen for iPB rheology. We acknowledge funding from the EPSRC (EP/P005403/1) and the Royal Commission for the Exhibition of 1851 and access to University of Nottingham High Performance Computing and HPC Midlands+ (EPSRC grant No. EP/P020232/1).

[1] A. Keller and H. W. Kolnaar, in *Processing of Polymers*, edited by H. Meijer (Wiley, Weinheim, 1997).
[2] F. L. Binsbergen, Nature **211**, 516 (1966).
[3] S. Kimata *et al.*, Science **316**, 1014 (2007).
[4] O. O. Mykhaylyk *et al.*, Macromolecules **41**, 1901 (2008).
[5] M. Seki *et al.*, Macromolecules **35**, 2583 (2002).
[6] G. Kumaraswamy, A. M. Issaian, and J. A. Kornfield, Macromolecules **32**, 7537 (1999).
[7] M. Stadlbauer *et al.*, J. Rheol. **48**, 631 (2004).
[8] E. E. Bischoff White, H. H. Winter, and J. P. Rothstein, Rheol Acta **51**, 303 (2012).
[9] R. Pantani *et al.*, Macromolecules **43**, 9030 (2010).
[10] F. G. Hamad, R. H. Colby, and S. T. Milner, Macromolecules **48**, 3725 (2015).
[11] Z. Wang *et al.*, Sci Rep **6**, 32968 (2016).
[12] K. Cui *et al.*, Chem. Rev. **118**, 1840 (2018).
[13] R. S. Graham, J Rheol **63**, 203 (2019).
[14] D. A. Nicholson and G. C. Rutledge, J. Chem. Phys. **145**, 244903 (2016).
[15] D. A. Nicholson and G. C. Rutledge, Journal of Rheology **63**, 465 (2019).
[16] M. Anwar, J. T. Berryman, and T. Schilling, J. Chem. Phys. **141**, 124910 (2014).
[17] M. Anwar and R. S. Graham, J. Chem. Phys. **150**, 084905 (2019).
[18] A. Jabbarzadeh, Nanomaterials **9** (2019).
[19] A. Jabbarzadeh and B. Halfina, Nanoscale Advances **1**, 4704 (2019).
[20] A. Doufas, I. Dairanieh, and A. McHugh, Journal of Rheology **43**, 85 (1999).
[21] S. Coppola *et al.*, Polymer **45**, 3249 (2004).
[22] R. J. A. Steenbakkers and G. W. M. Peters, J Rheol **55**, 401 (2011).
[23] P. C. Roozemond *et al.*, J Rheol **59**, 613 (2015).
[24] C. McIlroy and R. S. Graham, Additive Manufacturing **24**, 323 (2018).
[25] R. S. Graham and P. D. Olmsted, Phys Rev Lett **103**, 115702 (2009).
[26] R. S. Graham and P. D. Olmsted, Faraday Discuss **144**, 71 (2010).
[27] K. Jolley and R. S. Graham, Rheol.Acta **52**, 271 (2013).
[28] V. A. H. Boudara *et al.*, Journal of Rheology **63**, 71 (2019).
[29] See EPAPS Document No. XXXXX.
[30] M. J. Hamer, J. A. D. Wattis, and R. S. Graham, J Non-Newton Fluid Mech **165**, 1294 (2010).
[31] Available at http://reptate.readthedocs.io.
[32] S. Acierno *et al.*, Rheologica Acta **42**, 243 (2003).
[33] W. Schneider, A. Köppl, and J. Berger, Int. Polym. Proc. II **3**, 151 (1988).
[34] M. Yamashita and S. Ueno, Crystal Research and Technology **42**, 1222 (2007).

Supplementary information: The polySTRAND model of flow-induced nucleation in polymers

Daniel J. Read[1], Claire McIlroy[2,3], Chinmay Das[1], Oliver G. Harlen[1] and Richard S. Graham[3].

[1]School of Mathematics, University of Leeds, Leeds LS2 9JT, UK.

[2]School of Mathematics and Physics, University of Lincoln, Lincoln, UK, LN6 7TS

[3]School of Mathematical Sciences, University of Nottingham, Nottingham NG7 2RD, UK.

February 14, 2020

Nomenclature

Abbreviations

- FIC Flow-induced crystallisation
- FIN Flow-induced nucleation
- GO Graham and Olmsted model
- iPP Isotactic polypropylene
- iPB Isotactic poly-1-butene
- MD Molecular dynamics
- MWD Molecular weight distribution
- PDI Polydispersity index
- RDP Rolie-Double-Poly model

Symbols

- ϵ_B Bulk free energy gain of crystallisation
- γ Shear strain
- $\dot{\gamma}$ Shear rate
- Γ Prefactor relating free energy change to nematic order
- θ_i Volume fraction after local chain depletion
- κ Nucleus roughness penalty
- κ_0 Nucleus roughness penalty parameter
- μ_S Nucleus surface free energy
- ϕ_i Melt volume fraction
- ρ_K Kuhn segment density
- τ_e Rouse time of an entanglement segment
- τ_0 Monomer attachment time
- $\mathbf{A}$ Chain configuration tensor (Rolie-Double-Poly model)
- A, B Lagrange multipliers
- Δf_i Monomer free energy change under deformation
- F Nucleus free energy
- $F^{\mathrm{q}}_{\mathrm{GO}}$ Free energy from an exact quiescent calculation with the GO model
- F_{pS} Free energy from the polySTRAND model
- ΔF Change in free energy $[F(N_T) - F(0)]$
- ΔF^*_q Quiescent nucleation barrier height
- G_c Crystal growth rate
- $k^{+/-}_{st}$ Stem attachment/ detachment rate
- l Stem length
- L Average stem length
- M_e Molecular weight between entanglements
- M_n Number average molecular weight
- M_w Weight average molecular weight
- n^* Quiescent critical nucleus size in monomers
- $\dot{N}$ Nucleation rate
- N_0 Heterogeneous nucleation density
- N_e Kuhn steps between entanglements
- N_S Number of strands
- N_T Number of monomers
- P Average Δf_i, over the nucleus stem fraction w_i
- $P_{2,K}$ Kuhn step nematic order
- q Ratio of number of stems to monomers
- Q_S Number of stems a nucleus can draw from
- Q_{S0} Prefactor relating Q_S to the number of nucleus stems
- S Nucleus surface area
- T Temperature
- $t_{1/2}$ Turbidity half-time
- t_s Shearing time
- U_{nuc} Nucleus potential
- v_i Nucleus monomer fraction
- w_i Nucleus stem fraction

This nomenclature covers quantities that are referred to throughout the main manuscript and this Supplementary Information. Some other quantities are used only within a single derivation in this Supplementary Information. Such quantities are not included in the nomenclature and, instead, are defined locally in the relevant derivation.

1 Derivation of the polySTRAND model

Herein, we develop a thermodynamic approach that provides a nearly analytic method to compute the nucleation barrier, from the co-operative effect of different chain species in a flowing polymer melt. We name our model the POLYdisperse STRain Accelerated Nucleation Dynamics (polySTRAND) model, from which we derive two sub-models: the first (GO-polySTRAND) closely captures the GO model [4, 5] and the second (smooth-polySTRAND) adds extra physics required to capture experiments.

As an aside we note that the Free Energy calculations in sections 1 and 2 make use of a variety of (mostly) undergraduate methods: microcanonical and canonical ensemble; Lagrange multipliers for constrained minimisation; and Gaussian integration in the complex plane. There is scope for this to be the basis of an undergraduate project, for example.

1.1 Free Energy for the GO model

Consider a set of polymer species (polymer stems) i present at fraction ϕ_i in the melt. Let $k_BT\Delta f_i$ be the extra reduction in free energy of monomer addition to a growing nucleus due to chain deformation of species i. Let N_{Si} denote number of stems and N_{Ti} the number of monomers of type i in the nucleus, whilst N_S and N_T denote the total number of stems and monomers respectively. Then the entropic free-energy contribution, F_N, from arrangement of stems and monomers in the nucleus is given by

$$\frac{F_N}{k_BT} = -\log W_s - \sum_i \log W_i. \tag{1}$$

Here, W_s is the number of ways of arranging the N_{Si} stems of each species amongst the total N_S stems:

$$W_s = \frac{N_S!}{\prod_i N_{Si}!}.$$

W_i is number of ways of arranging N_{Ti} monomers amongst N_{Si} stems,

$$W_i = \frac{(N_{Ti}-1)!}{(N_{Ti}-N_{Si})!((N_{Si}-1)!}.$$

Provided $N_{Si} \gg 1$ we can approximate both using Stirling's formula so that at leading order

$$\log W_s \approx N_S \log N_S - \sum_i N_{Si} \log N_{Si},$$
$$\log W_i \approx N_{Ti} \log N_{Ti} - (N_{Ti}-N_{Si}) \log(N_{Ti}-N_{Si}) - N_{Si} \log N_{Si}.$$

Now define w_i and v_i to be, respectively, the proportion of total stems and segments, such that

$$N_{Si} = w_i N_S, \qquad N_{Ti} = v_i N_T,$$

where $\sum w_i = \sum v_i = 1$. Then $\log W_s$ and $\log W_i$ can be rewritten as:

$$\log W_s = -N_S \sum_i w_i \log w_i$$
$$\log W_i = N_T \left(v_i \log v_i - (v_i - qw_i)\log(v_i - qw_i) - qw_i \log(qw_i)\right),$$

where $q = N_S/N_T$.

Hence free energy contribution from arrangements can be written as

$$F_N = k_BTN_T \sum_i \left[2qw_i \log(w_i) + (v_i - qw_i)\log(v_i - qw_i) - v_i \log v_i\right] + k_BTN_S \log q. \tag{2}$$

To this we need to add: the free energy from choosing stems from the bulk at volume fraction ϕ_i (where $\log \phi_i$ gives the effective stem chemical potential - see section 2.1 below):

$$F_A = -k_BT \sum_i N_{Si} \log \phi_i = -k_BTN_T \sum_i qw_i \log \phi_i; \tag{3}$$

and the modification of monomer attachment free energy due to chain stretching of each species i

$$F_S = -\sum_i N_{Ti} k_BT \Delta f_i = -k_BTN_T \sum_i v_i \Delta f_i; \tag{4}$$

and the quiescent potential for formation the nucleus $U_{\rm nuc}/k_BT = -\epsilon_B N_T + \mu_S S(N_T, N_S)$, where ϵ_B is the bulk energy reduction from crystallising a monomer from the isotropic melt (in units of k_BT), μ_S is the surface energy per unit area (also in units of k_BT), and S is the surface area of the ellipsoid nucleus. Hence the total free energy is given by

$$\begin{aligned}\frac{F(N_T, N_S, \{w_i\}, \{v_i\})}{k_BT} = N_T \sum_i [qw_i(2\log w_i - \log\phi_i) - v_i \log v_i + (v_i - qw_i)\log(v_i - qw_i) - v_i\Delta f_i] \\ + N_S \log q - \epsilon_B N_T + \mu_S S(N_T, N_S).\end{aligned} \tag{5}$$

Hence the free-energy can be divided into a term, $F_{\rm all}$ that depends only on N_T and N_S and a sum over the different modes as

$$F = k_BTF_{\rm all} + k_BTN_T \sum_i E_i, \tag{6}$$

where

$$F_{\rm all} = N_S \log q - \epsilon_B N_T + \mu_S S(N_T, N_S), \tag{7}$$

and

$$E_i = qw_i(2\log w_i - \log\phi_i) - v_i \log v_i + (v_i - qw_i)\log(v_i - qw_i) - v_i\Delta f_i. \tag{8}$$

1.2 Solving for v_i and w_i

To find the distributions v_i and w_i for a given N_T and N_S we need to minimize $F(N_T, N_S, \{w_i\}, \{v_i\})$ subject to the constraints that $\sum w_i = \sum v_i = 1$, which we impose by introducing Lagrange multipliers α and β respectively, to give

$$\frac{\partial E_i}{\partial v_i} = -\log v_i + \log(v_i - qw_i) - \Delta f_i = \alpha, \tag{9}$$

$$\frac{\partial E_i}{\partial w_i} = 2q\log w_i - q\log\phi_i - q\log(v_i - qw_i) + q = \beta. \tag{10}$$

Rearranging equation (9) gives a relationship between v_i and w_i as

$$v_i = \frac{q}{1 - A\exp(\Delta f_i)} w_i, \tag{11}$$

for some constant A, given by the condition

$$q\sum_i \frac{w_i}{1 - A\exp(\Delta f_i)} = 1. \tag{12}$$

Therefore

$$\log(v_i - qw_i) = \log\left(\frac{qA\exp(\Delta f_i)}{1 - A\exp(\Delta f_i)}\right) + \log w_i.$$

Substituting this into equation (10) and using $\sum w_i = 1$ gives

$$w_i = B\frac{\phi_i \exp(\Delta f_i)}{1 - A\exp(\Delta f_i)}, \tag{13}$$

where

$$B = \left[\sum_i \left(\frac{\phi_i \exp(\Delta f_i)}{1 - A\exp(\Delta f_i)}\right)\right]^{-1}. \tag{14}$$

Hence from equation(11),

$$v_i = B\frac{q\phi_i \exp(\Delta f_i)}{(1 - A\exp(\Delta f_i))^2}, \tag{15}$$

where A is the solution of

$$q\sum_i \frac{\phi_i \exp(\Delta f_i)}{(1 - A\exp(\Delta f_i))^2} = \sum_i \frac{\phi_i \exp(\Delta f_i)}{1 - A\exp(\Delta f_i)}. \tag{16}$$

This non-linear equation can be solved numerically to find A, and thence B from Eq. (14). The values of w_i and v_i are then obtained from equations (13) and (15).

Note that in the case where Δf_i are all equal then equations (13) and (15) simply reduce to $w_i = v_i = \phi_i$. However, when Δf_i are not equal, the fraction of stems of mode i in the nucleus is enhanced by a factor,

$$\frac{\exp(\Delta f_i)}{1 - A\exp(\Delta f_i)},$$

while the number of segments is enhanced by a further factor of $1 - A\exp(\Delta f_i)$ in the denominator meaning that the average length of attached stems is also longer.

Having obtained v_i and w_i, which minimise the free energy, these values can be substituted back into $F(N_T, N_S, \{w_i\}, \{v_i\})$ from Eq. (5) to obtain the free energy as a function of N_T and N_S. We name this sub-model the GO-polySTRAND model.

1.3 Computing a 1D nucleation barrier

We require 1D nucleation barriers from the GO-polySTRAND model in order to compare with GO model simulations and to compute the nucleation rate via a 1D Kramer's calculation (see section 3 below). We compute this 1D barrier as follows. We use the GO-polySTRAND model to calculate the free energy for a given number of monomers and stems, $F(N_T, N_S)$. Then, for a given N_T we numerically minimise this over N_S to give N_S^* the optimum number of strands (for the given N_T value). Next, we account for leading order fluctuations about N_S^* using

$$F_{\rm pS}(N_T) = F(N_T, N_S^*) + \ln\left(\frac{1}{2\pi}\frac{\partial^2 F}{\partial N_S^2}\bigg|_{N_S=N_S^*}\right), \tag{17}$$

where we compute $\frac{\partial^2 F}{\partial N_S^2}$ via the standard central difference expression. We use the same method to compute $F_{\rm pS}^{\rm q}$, the GO-polySTRAND model barrier for undeformed chains. Finally, we compute the change in the barrier due to chain deformation, $F_{\rm pS}^{\rm q} - F_{\rm pS}$ and subtract this from a full calculation of the quiescent GO model barrier, $F_{\rm GO}^{\rm q}$ [5] to give the overall nucleation barrier,

$$F_{\rm final}(N_T) = F_{\rm GO}^{\rm q}(N_T) - \Big(F_{\rm pS}^{\rm q}(N_T) - F_{\rm pS}(N_T)\Big), \tag{18}$$

The quiescent GO model barrier can be readily and cheaply computed from the nearly analytic algorithm in Appendix A of Jolley and Graham [8].

1.4 Comparison with GO Monte Carlo simulations

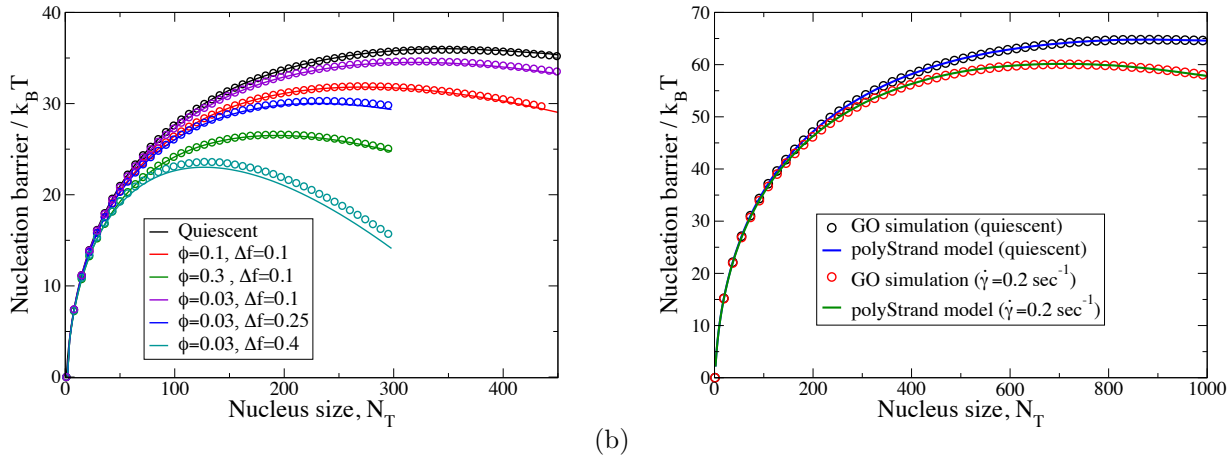

(a) (b)

Figure 1: Comparison of direct Monte Carlo simulations from the GO model (symbols) and calculations of the GO-polySTRAND model (lines) (Eq. 18). (a) Bimodal blends where the first component has volume fraction ϕ and extra free energy reduction Δf, as specified in the legend and the second component is undeformed. (b) The nucleation barrier used for the comparison with iPP experiments at $\dot\gamma = 0.2$ sec^{-1} and 138°C (see figure 3 in the main article)

The GO-polySTRAND model is intended to be a fast method to predict the nucleation barrier under flow in the GO simulation algorithm. The model can be tested by direct comparison to simulated nucleation barriers from GO model simulations. We extensively tested the GO-polySTRAND model's predictions (equation 18) in this way and we report a sample of typical results here. We found that bimodal blends in which one species is undeformed ($\Delta f = 0$)

and the other is strongly stretched, are the most challenging. Here, the wide separation of the Δf creates significant over-representation of long chains in the nucleus and the barriers are sensitive to this over-representation. We ran Monte-Carlo simulations of nucleation barriers in the GO model, using the algorithm of Jolley and Graham [7], for bimodal blends with long chains at a volume fraction ϕ and extra free energy reduction Δf and with undeformed short chains at volume fraction (1-ϕ). These simulated barriers are compared with the GO-polySTRAND model predictions in figure 1(a). The GO-polySTRAND model generally captures the overall barrier very accurately across the whole barrier. A notable exception is the lowest barrier in figure 1(a) where the predicted barrier is slightly lower than the simulated barrier. This case has a low fraction of very highly deformed chains, leading to a very strong barrier reduction. Two potential reasons for this slight disagreement are inaccuracy of Stirling's approximation and the neglect of fluctuations in the nucleus composition, which are likely more important when the barrier is dominated by rare highly deformed chains.

2 The smooth-polySTRAND model

2.1 Nucleation from a finite supply of stems

The above calculation assumes that a nucleus grows from an infinite supply of stems from the melt, present at fractions $\{\phi_i\}$. However, it is possible that the supply of stems is kinetically limited: during a nucleation event the nucleus has access only to a limited number of stems. Let us suppose that the N_S stems in a growing nucleus are chosen from an initial supply of Q_S stems in the melt with initial fraction ϕ_i of species i. If stems are present in the nucleus at fraction w_i, this leaves a remaining $Q_S - N_S$ stems with species i present at fraction θ_i, where conservation of the number of stems in each species gives

$$(Q_S - N_S)\theta_i + N_S w_i = Q_S \phi_i. \tag{19}$$

The entropic free energy of arrangements of stems at fraction w_i in the nucleus is already calculated above. There remains the change in free energy from re-arrangements of stems in the initial melt (Q_S stems at fraction ϕ_i) and the depleted melt ($Q_S - N_S$ stems at fraction θ_i). This is obtained from the change in entropy of arrangements, giving:

$$F_A/k_BT = (Q_S - N_S)\sum_i \theta_i \log\theta_i - Q_S \sum_i \phi_i \log\phi_i. \tag{20}$$

This replaces the free energy contribution from Eq. 3 above and, in the limit $Q_S \to \infty$, Eq. 20 reduces to Eq. 3 (which confirms the effective chemical potential used there).

With this contribution, the free energy becomes:

$$\begin{aligned}\frac{F(N_T, N_S, \{w_i\}, \{v_i\})}{k_BT} = N_T \sum_i [&2qw_i \log w_i - v_i \log v_i + (v_i - qw_i)\log(v_i - qw_i) - v_i \Delta f_i] \\ &+ (Q_S - N_S)\sum_i \theta_i \log\theta_i - Q_S \sum_i \phi_i \log\phi_i \\ &+ N_S \log q - \epsilon_B N_T + \mu_S S(N_T, N_S).\end{aligned} \tag{21}$$

We now proceed as with the GO-polySTRAND model by locating the chemical equilibrium between the nucleus and the locally surrounding melt. One can proceed again by minimising this free energy to obtain w_i and v_i as before. However, a quick route to the answer is to recognise that the remaining $(Q_S - N_S)$ stems at fractions θ_i would be in equilibrium with a hypothetical infinite melt also at fraction θ_i (and both would be in equilibrium with the nucleus). Hence the previous analysis holds with ϕ_i replaced by θ_i, and equations (13) and (15) become:

$$w_i = B\frac{\theta_i \exp(\Delta f_i)}{1 - A\exp(\Delta f_i)}, \tag{22}$$

$$v_i = B\frac{q\theta_i \exp(\Delta f_i)}{(1 - A\exp(\Delta f_i))^2}. \tag{23}$$

Substituting from Eq. (22) into Eq. (19) and rearranging gives:

$$\theta_i = \frac{Q_S \phi_i}{Q_S + N_S\left(\frac{B\exp(\Delta f_i)}{1 - A\exp(\Delta f_i)} - 1\right)}, \tag{24}$$

and substituting this in turn into Eqs. (22) and (23) and requiring that $\sum w_i = \sum v_i = 1$ gives a pair of non-linear

equations for A and B:

$$B\sum_i \frac{Q_S\phi_i \exp(\Delta f_i)}{\left[Q_S + N_S\left(\frac{B\exp(\Delta f_i)}{1-A\exp(\Delta f_i)} - 1\right)\right][1 - A\exp(\Delta f_i)]} = 1, \tag{25}$$

$$Bq\sum_i \frac{Q_S\phi_i \exp(\Delta f_i)}{\left[Q_S + N_S\left(\frac{B\exp(\Delta f_i)}{1-A\exp(\Delta f_i)} - 1\right)\right][1 - A\exp(\Delta f_i)]^2} = 1. \tag{26}$$

Solution of these yields A and B, thence θ_i (Eq. 24), w_i (Eq. 22) and v_i (Eq. 23). These values can be substituted back into $F(N_T, N_S, \{w_i\}, \{v_i\})$ from Eq. (21) to obtain the free energy as a function of N_T and N_S only. For a given N_T, this may be numerically minimised over N_S to obtain the free energy as a function of N_T only, which yields the form of the crystallisation nucleation barrier, once fluctuations in N_S are accounted for in the same way as in the GO-polySTRAND model (Eq. 17). The above derivations corresponds to locating the chemical equilibrium between the nucleus and the locally surrounding melt (which minimizes the total free energy of both). Hence the GO-polyStrand and smooth-polyStrand models are derived by exactly the same method. The difference is that the GO-Polystrand model locates equilibrium with the infinite melt and the smooth-polyStrand locates equilibrium with a finite region of melt.

2.2 Free energy of a nucleus with surface roughness penalty

We now consider an approximate model that penalises large deviations of stem length from the average. We assume that deviations between number of monomers l in a stem and the nucleus average $L = N_T/N_S = 1/q$ are penalised via an energy (in units of k_BT) of $\frac{1}{2}\kappa(l-L)^2$ per stem. Together with the extra free energy per monomer $-k_BT\Delta f_i$, the energy for stem α from stem type i is:

$$\frac{E_\alpha}{k_BT} = \frac{1}{2}\kappa(l_\alpha - L)^2 - l_\alpha\Delta f_{i,\alpha}.$$

For a nucleus containing N_S stems and N_T monomers, with N_{Si} stems of type i, we can write the partition function by summing over all possible lengths of each stem subject to the constraint of the total number of monomers:

$$Z = W_s \sum_{l_1}\sum_{l_2}\sum_{l_3}\cdots\sum_{l_{N_S}} \delta_{N_T - \sum_\alpha l_\alpha} \prod_i \prod_{\alpha\in i} \exp\left(-\frac{1}{2}\kappa(l_\alpha - L)^2 + l_\alpha\Delta f_{i,\alpha}\right), \tag{27}$$

where, as in section 1.1, W_s is the number of ways of arranging the N_{Si} stems of each species amongst the total N_S stems:

$$W_s = \frac{N_S!}{\prod_i N_{Si}!}.$$

We approximate the sums over monomers in Eq. (27) by integrals, and for sufficiently large κ we take the limits to infinity (since the integrals will be dominated by l close to L):

$$Z = W_s \int_{-\infty}^{\infty}\mathrm{d}l_1\int_{-\infty}^{\infty}\mathrm{d}l_2\int_{-\infty}^{\infty}\mathrm{d}l_3\ldots\int_{-\infty}^{\infty}\mathrm{d}l_{N_S}\delta(N_T - \sum_\alpha l_\alpha)\prod_i\prod_{\alpha\in i}\exp\left(-\frac{1}{2}\kappa(l_\alpha - L)^2 + l_\alpha\Delta f_{i,\alpha}\right), \tag{28}$$

and then replace the delta-function by a Fourier integral:

$$\delta(N_T - \sum_\alpha l_\alpha) = \frac{1}{2\pi}\int_{-\infty}^{\infty}\mathrm{d}J\exp\left[iJ\left(N_T - \sum_\alpha l_\alpha\right)\right].$$

Reversing the order of integration and collecting together the integrals over lengths of stem of the same type gives:

$$Z = W_s\frac{1}{2\pi}\int_{-\infty}^{\infty}\mathrm{d}J\exp(iJN_T)\prod_i\left[\int_{-\infty}^{\infty}\mathrm{d}l\exp\left(-\frac{1}{2}\kappa(l-L)^2 + \Delta f_i l - iJl\right)\right]^{N_{Si}}. \tag{29}$$

Writing $N_{Si} = w_iN_S$, and performing Gaussian integrals over l and J gives, finally:

$$Z = W_s\left(\frac{2\pi}{\kappa}\right)^{(N_S-1)/2}\frac{1}{\sqrt{N_S}}\exp\left[N_T\mathrm{E}(\Delta f) + \frac{N_S}{2\kappa}\mathrm{Var}(\Delta f)\right], \tag{30}$$

where

$$\mathrm{E}(\Delta f) = \sum_i w_i\Delta f_i,$$

$$\mathrm{Var}(\Delta f) = \sum_i w_i\Delta f_i^2 - \left(\sum_i w_i\Delta f_i\right)^2$$

are the mean and variance of Δf_i over the distribution w_i.

To calculate the nucleus free energy we use $F = -k_B T \log Z$ and add the quiescent potential for formation of the nucleus $U_{\text{nuc}}/k_B T = -\epsilon_B N_T + \mu_S S(N_T, N_S)$, together with free energy of drawing stems from the surrounding melt using either Eq. (3) or Eq. (20) depending upon whether we consider a finite supply of stems. We deal with each case in turn.

2.2.1 Infinite stem supply

We use Eq. (3) for F_A, giving free energy:

$$\begin{aligned}\frac{F(N_T, N_S, w_i)}{k_B T} &= N_S \sum_i w_i(\log w_i - \log \phi_i) - N_T \mathrm{E}(\Delta f) - (N_S/2\kappa)\mathrm{Var}(\Delta f) + \tfrac{1}{2}\log N_S \\ &\quad - \tfrac{1}{2}(N_S - 1)\log(2\pi/\kappa) - \epsilon_B N_T + \mu_S S(N_T, N_S).\end{aligned} \tag{31}$$

Note that this depends on w_i but not v_i, since in this derivation we have summed over all stem lengths to calculate the partition function. Following the same methods as in section 1.2 we minimise over the w_i subject to constraint $\sum w_i = 1$, imposed via Lagrange multiplier λ:

$$\frac{1}{k_B T N_s}\frac{\partial F}{\partial w_i} = \log w_i - \log \phi_i + 1 - L\Delta f_i - \frac{1}{2\kappa}\Delta f_i^2 + \frac{1}{\kappa}\mathrm{E}(\Delta f)\Delta f_i = \lambda, \tag{32}$$

which rearranges to give:

$$w_i = A\phi_i \exp\left(L\Delta f_i + \frac{1}{2\kappa}\Delta f_i^2 - \frac{\Delta f_i}{\kappa}P\right) \tag{33}$$

for some constant A and where $P = \mathrm{E}(\Delta f)$. The constant A satisfies normalisation condition $\sum w_i = 1$ and so

$$w_i = \frac{\phi_i \exp\left(L\Delta f_i + \frac{1}{2\kappa}\Delta f_i^2 - \frac{\Delta f_i}{\kappa}P\right)}{\sum_i \phi_i \exp\left(L\Delta f_i + \frac{1}{2\kappa}\Delta f_i^2 - \frac{\Delta f_i}{\kappa}P\right)}. \tag{34}$$

But, $P = \sum_i w_i \Delta f_i$ depends on the w_i, so we have a self consistent formula for P:

$$P = \frac{\sum_i \Delta f_i \phi_i \exp\left(L\Delta f_i + \frac{1}{2\kappa}\Delta f_i^2 - \frac{\Delta f_i}{\kappa}P\right)}{\sum_i \phi_i \exp\left(L\Delta f_i + \frac{1}{2\kappa}\Delta f_i^2 - \frac{\Delta f_i}{\kappa}P\right)}. \tag{35}$$

Numerical solution of the non-linear equation (35) for P allows the w_i to be calculated from Eq. (34). Substitution into Eq. (31) gives the free energy as a function of N_T and N_S only. For a given N_T, this may be numerically minimised over N_S to obtain the free energy as a function of N_T only, which yields the form of the crystallisation nucleation barrier.

2.2.2 Finite stem supply

Instead we use Eq. (20) for F_A, giving free energy:

$$\begin{aligned}\frac{F}{k_B T} &= \sum_i [(Q_S - N_S)\theta_i \log \theta_i - Q_S \phi_i \log \phi_i + N_S w_i \log w_i] \\ &\quad - N_T \mathrm{E}(\Delta f) - (N_S/2\kappa)\mathrm{Var}(\Delta f) + \tfrac{1}{2}\log N_S \\ &\quad - \tfrac{1}{2}(N_S - 1)\log(2\pi/\kappa) - \epsilon_B N_T + \mu_S S(N_T, N_S).\end{aligned} \tag{36}$$

where, as in Section 2.1,

$$(Q_S - N_S)\theta_i + N_S w_i = Q_S \phi_i. \tag{37}$$

Following the same arguments as in section 2, we note that the nucleus is effectively in equilibrium with melt at composition θ_i, and so we replace ϕ_i with θ_i in Eq. (33) giving

$$w_i = A\theta_i \exp\left(L\Delta f_i + \frac{1}{2\kappa}\Delta f_i^2 - \frac{\Delta f_i}{\kappa}P\right)$$

for some A, which rearranges to:

$$\theta_i = B w_i \exp\left(-L\Delta f_i - \frac{1}{2\kappa}\Delta f_i^2 + \frac{\Delta f_i}{\kappa}P\right)$$

for $B = 1/A$. Substituting back into Eq. (37) and rearranging gives:

$$w_i = \frac{Q_S \phi_i}{N_S + B(N_S - Q_S)\exp\left(-L\Delta f_i - \frac{1}{2\kappa}\Delta f_i^2 + \frac{\Delta f_i}{\kappa}P\right)}. \tag{38}$$

The constraints $\sum w_i = 1$ and $P = \sum_i w_i \Delta f_i$ give a pair of non-linear equations that can be solved to yield P and B:

$$\sum_i \frac{Q_S \phi_i}{N_S + B(N_S - Q_S)\exp\left(-L\Delta f_i - \frac{1}{2\kappa}\Delta f_i^2 + \frac{\Delta f_i}{\kappa}P\right)} = 1, \tag{39}$$

$$\sum_i \frac{Q_S \phi_i \Delta f_i}{N_S + B(N_S - Q_S)\exp\left(-L\Delta f_i - \frac{1}{2\kappa}\Delta f_i^2 + \frac{\Delta f_i}{\kappa}P\right)} = P. \tag{40}$$

Substitution into Eq. (38) gives the w_i. Substitution of these into Eq. (36) gives the free energy as a function of N_T and N_S only. For a given N_T, this may be numerically minimised over N_S to obtain the free energy as a function of N_T only, which yields the form of the crystallisation nucleation barrier. We account for fluctuations in N_S is the same way as the GO-polySTRAND model (see equation 17). We name this sub-model the smooth-polySTRAND model.

3 Calculating the Nucleation Rate

Having computed the nucleation barrier from the polySTRAND model $F(N_T)$, as detailed above, we now compute the nucleation rate via a barrier crossing calculation. Hamer *et al.* [6] developed a method to project the kinetics of the GO simulation algorithm onto a 1D Kramer's problem that can be solved analytically. This approach was found to predict well the barrier crossing kinetics for both quiescent and flow induced nucleation simulations of the GO model [6, 8]. We adopt this 1D projection approach for both the GO-polySTRAND and smooth-polySTRAND models, as outlined below. In the following derivation, all free energies are in units of $k_B T$ and we use $\Delta F(N_T) = F(N_T) - F(0)$, that is, the free energy difference of a nucleus of size N_T relative to the melt ($N_T = 0$).

For the 1D projection we require the nucleation barrier $F(N_T)$ (in units of $k_B T$), as computed above, and the effective surface area of monomer attachment/detachment, $A(N_T)$ for a nucleus of N_T monomers. If both are known then, a 1D analogue of Kramer's problem [6], gives a recurrence relation for the average first passage time $< t_F >$ to achieve a nucleus of size N_T,

$$< t_F >_{N_T+1} = < t_F >_{N_T} + \frac{\exp(\Delta F(N_T))}{r^+(N_T)} \sum_{i=1}^{N_T} \exp(-\Delta F(i)), \tag{41}$$

where $r^+(N_T)$ is the rate of adding a single monomer to a nucleus of size N_T,

$$r^+(N_T) = \frac{1}{\tau_0} \min\left[1, \exp(\Delta F(N_T) - \Delta F(N_T + 1)\right] A(N_T). \tag{42}$$

Here τ_0 is the timescale for monomer attachment/detachment. Hamer *et al.* [6] showed that the following expression for the surface area captures well the nucleation rates from the GO model,

$$A(N_T) = 2(n^*)^{2/3} \left(\frac{N_T}{n^*}\right)^{\alpha}, \tag{43}$$

where n^* is the critical nucleus size and $\alpha = 0.8$. There is an exact solution to the recurrence relation (equation 42) [6], but for barriers heights above a few $k_B T$ this can be approximated by the much cheaper direct formula for the average nucleation time

$$< t_F > = \kappa_{\text{nuc}} \exp\left(\Delta F^*\right), \tag{44}$$

where ΔF^* is the nucleation barrier height and κ_{nuc} is a kinetic pre-factor, given by,

$$\kappa_{\text{nuc}} = \frac{\tau_0}{2{n^*}^{2/3}} \left[1 + \sqrt{-\frac{2\pi}{F''(n^*)}} \exp\left(\frac{-\alpha^2}{2{n^*}^2 F''(n^*)} + \frac{\alpha}{n^*}\right)\right] \sum_{i=0}^{n^*} \exp(-\Delta F(i)). \tag{45}$$

Here $F''(n^*)$ is the curvature of the nucleation barrier at its peak, which we compute by the standard central difference expression. The sum in equation 45 is dominated by the barrier base and so only requires the first few terms. Finally, the nucleation rate is given by

$$\dot{N} = \frac{1}{< t_F >}. \tag{46}$$

The kinetic pre-factor, κ_{nuc}, changes only slightly due to flow. Thus, for a given system, we compute the quiescent nucleation rate $\dot{N}_q$ with equation 45 and approximate the flow induced nucleation rate, $\dot{N}_\Lambda$ by

$$\dot{N}_\Lambda = \dot{N}_q \exp(\Delta F_q^* - \Delta F_\Lambda^*), \tag{47}$$

where ΔF_Λ^* is the height of the nucleation barrier under flow (as computed by the polySTRAND model).

Nucleation rates from our models are rates per Kuhn step, whereas experiments measure the rate per unit volume. Hence we compare to experiments via the expression

$$\dot{N}^{\text{experiment}} = \rho_K \dot{N}_\Lambda, \tag{48}$$

where ρ_K is the Kuhn step density.

4 Obtaining Model Parameters

The model consists of parameters divided into four classes; material, rheological, quiescent nucleation, and FIN. Here we describe the steps needed to obtain these model parameters. Importantly, material, rheological and quiescent parameters are obtained from experimentally measured material characterisation in the absence of non-linear flow. The small number of FIC parameters are independent of MWD and temperature, and are chosen by fitting FIC experiments, for a single MWD and temperature. We discuss how the parameters are obtained to achieve the predictions shown in Fig.2; Tables 1 & 3 give a list of parameters.

4.1 Parameter Classification

1. **Material parameters**

   First we require fundamental properties of the material. The Kuhn molecular weight is given by $M_K = M_{\text{mono}} C_\infty$, where M_{mono} is the monomer molecular weight and C_∞ is the characteristic ratio, available in the literature. Then, the Kuhn step density is given by

   $$\rho_K = \frac{\rho_a N_A}{M_K}, \tag{49}$$

   where ρ_a is the density of the amorphous polymer. The Kuhn step density is required in Eq.48 for the polySTRAND model. The crystal growth rate G_c can usually be obtained from the literature.

2. **Rheological parameters**

   We require the tube model parameters to predict the non-linear flow of each sample via Rolie-Double-Poly (RDP) [2]; this enables prediction of the order parameter $P_{2,K}$ and thus the elastic energy Δf required in the polySTRAND model. The entanglement molecular weight M_e and the entanglement relaxation time τ_e are obtained by fitting a linear viscoelastic (LVE) model to linear oscillatory shear measurements with knowledge of the MWD from GPC. We choose either the Branch-on-Branch (BoB) hierarchical model [3], or the linear RDP model [2]. Both are implemented in RepTate software[1]. The plateau modulus is not an independent parameter and, instead, is specified by the relation

   $$G_N = \frac{4\rho_a RT}{5M_e}. \tag{50}$$

   Usually GPC and LVE measurements are available in the literature. Since M_e is specified by the length of the rubbery plateau in LVE measurements, accurate fitting requires high frequency data. Such high-frequency data are usually unavailable for crystallisable materials as crystallisation prevents extensive use of time-temperature superposition. In some materials τ_e depends weakly on MWD because of variations in the activation energy (see Table 2). The number of steps per entanglement segment is given by

   $$N_e = M_e/M_K, \tag{51}$$

   and appears in the order parameter $P_{2,K}$, and the monomer attachment time (Eq.53).

3. **Quiescent nucleation parameters**

   Predicting the FIN rate in the polySTRAND model requires knowledge of the quiescent nucleation kinetics (Sec.3). Required parameters are the monomer attachment rate τ_0, along with the shape of the quiescent nucleation barrier through the surface and bulk free energies, μ_S and ϵ_B, (or equivalently the critical nucleus size, n^* and the height of the quiescent barrier, ΔF_q^*). The critical nucleus size is estimated via

   $$n^* = \frac{M_{n^*}}{M_K}, \tag{52}$$

where the molar mass of the critical nucleus (assumed to be spherical) is $M_{n^*} = 4\pi\rho_c N_A r_l^3/3$, for lamella thickness $2r_l$ and crystal density ρ_c. By adjusting the free energy of crystallization per monomer, ϵ_B, and the surface energy cost, μ_S, the height of the quiescent barrier can be selected to give a quiescent nucleation rate, $\dot{N}_q$, equivalent to that measured experimentally. The monomer attachment time, τ_0, is given by projecting τ_e to the Kuhn step length scale:

$$\tau_0 \approx \tau_K = \frac{\tau_e}{N_e^2}. \tag{53}$$

All these parameters are independent of MWD. To change temperature, μ_s is held fixed and ϵ_B is varied to capture the change in quiescent nucleation rate, leading to changes in both ΔF_q^* and n^*

4. **FIC parameters**

The remaining parameters relate to FIC and are independent of MWD and temperature. The only FIC parameter in the GO-polySTRAND model is Γ, which determines the sensitivity of the monomer free energy to the nematic order parameter $P_{2,K}$. This should be of order 1 and can be fitted to experimental measurements at the onset of FIC. The smooth-polySTRAND model introduces two further FIC parameters κ_0, the nucleus roughness penalty and Q_{s0}, which determines the size of the region from which new strands can attach to the nucleus. All FIC parameters are independent of temperature and MWD.

Next we describe how the parameters are obtained to describe the FIN experiments on iPP (Fig.2(a)) and the FIC experiments on iPB (Fig.2(b)), respectively.

Parameter	Value	Method
Material Parameters		
ρ_K	$2.7\times10^9\mu\text{m}^{-3}$	Literature data and Eq. 49 (see ref [4])
G_c	N/A	Not required to model nucleation
Rheological Parameters		
M_e	4.4 kg mol^{-1}	Literature data and
τ_e	90 ns (at 140°C)	confirmed by linear rheology
N_e	25	(see ref [4])
Quiescent Nucleation Parameters		
τ_0	0.76 ns	Projected from τ_e (see ref [4])
GO-polySTRAND model		
μ_S	0.85	Adjusted (with ϵ_B) to capture $\dot{N}_q$ and n^* (Eq. 52) at $T = 140$°C
ϵ_B	-0.117 ($T = 140$°C)	Adjusted (with μ_S) to capture $\dot{N}_q$ and n^* (Eq. 52) at $T = 140$°C
	-0.118 ($T = 144$°C)	Adjusted to capture $\dot{N}_q$ at $T = 144$°C (with μ_S fixed)
	-0.01146 ($T = 138$°C)	Adjusted to capture $\dot{N}_q$ at $T = 138$°C (with μ_S fixed)
Smooth-polySTRAND model		
μ_S	0.94	Adjusted (with ϵ_B) to capture $\dot{N}_q$ and n^* (Eq. 52) at $T = 140$°C
ϵ_B	0.044 ($T = 140$°C)	Adjusted (with μ_S) to capture $\dot{N}_q$ and n^* (Eq. 52)at $T = 140$°C
	0.0429 ($T = 144$°C)	Adjusted to capture $\dot{N}_q$ at $T = 144$°C (with μ_S fixed)
	0.0463 ($T = 138$°C)	Adjusted to capture $\dot{N}_q$ at $T = 138$°C (with μ_S fixed)
FIC Parameters		
Γ	4.3	Fitted to low shear rate FIC data at $T = 140$°C only
κ_0	0.1	*Smooth-polySTRAND only*: Fitted to FIC data at $T = 140$°C only
Q_{s0}	30.0	*Smooth-polySTRAND only*: Fitted to FIC data at $T = 140$°C only

Table 1: Model parameters used to capture the experimentally measured flow-induced nucleation rate, $\dot{N}$, in iPP [10] using the polySTRAND model corresponding to results shown in Fig.2(a). The quiescent nucleation parameters give the same quiescent barrier for both the GO and smooth polySTRAND models.

4.2 FIN in iPP (Fig.2(a))

Since iPP has previously been studied in the context of modelling FIN, we refer the reader to Refs.[4, 8] for further detail; the material, rheological and quiescent parameters obtained from materials characterisation are listed in Table 1. Since GPC data is not available, we model the MWD as a generalized exponential distribution, as implemented in the RepTate software[1] with parameters selected to give the reported M_w and M_n. To obtain the FIN parameters we

[1]Available at http://reptate.readthedocs.io.

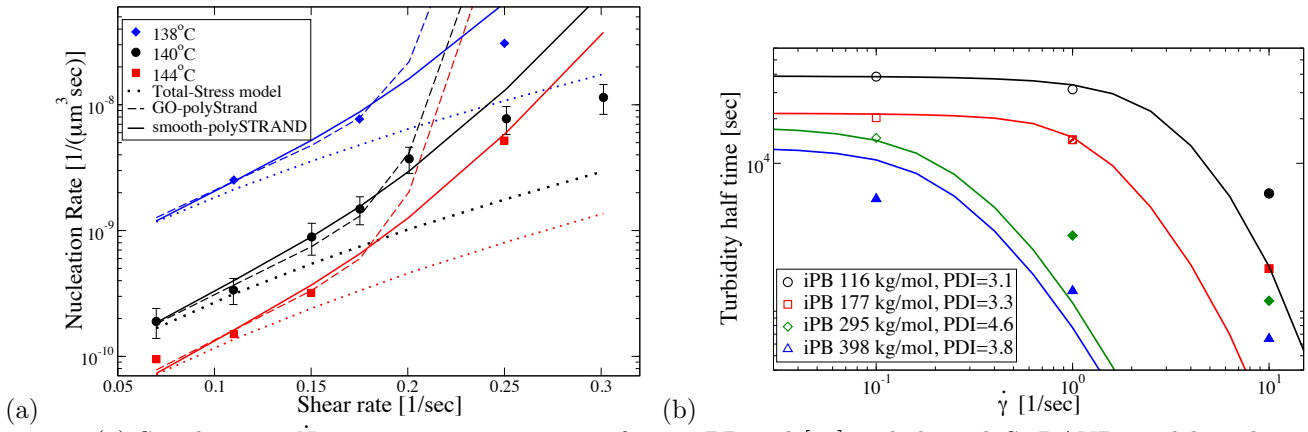

(a) (b)

Figure 2: (a) Steady-state $\dot{N}$ measurements against $\dot{\gamma}$ for an iPP melt[10] and the polySTRAND models. The total-stress model pre-averages chain deformation into a single species. (b) Experiments [1] and the smooth-polySTRAND model for $t_{1/2}$ after a shear of $\gamma = 60$ for iPB. The legend shows M_w and M_w/M_n (PDI). The open, closed and shaded symbols indicate spherical, rod and mixed morphologies, respectively.

adjusted the low-shear barrier height ΔF_q^* and Γ to capture the lowest two shear rates at 140°C, obtaining $65.0 k_B T$ and 4.3, respectively. We modelled the other temperatures by adjusting *only* ϵ_B to capture the lowest $\dot{\gamma}$, obtaining ΔF_q^* of 63.8 and $66.7 k_B T$ at 130, and 144°C, respectively. In Fig.2(a) a slight enhancement of the high-molecular weight tail was required to capture the curvature of the experiments with the polySTRAND model; we added a mode of mass 1.9×10^5 kg mol^{-1} at $\phi = 0.03\%$. For the smooth-polySTRAND we slightly increased the mass of the extra high-molecular weight mode to 3.0×10^5 kg mol^{-1}, and used $Q_{S0} = 30$ and $\kappa_0 = 0.1$.

4.3 FIC in iPB (Fig.2(b))

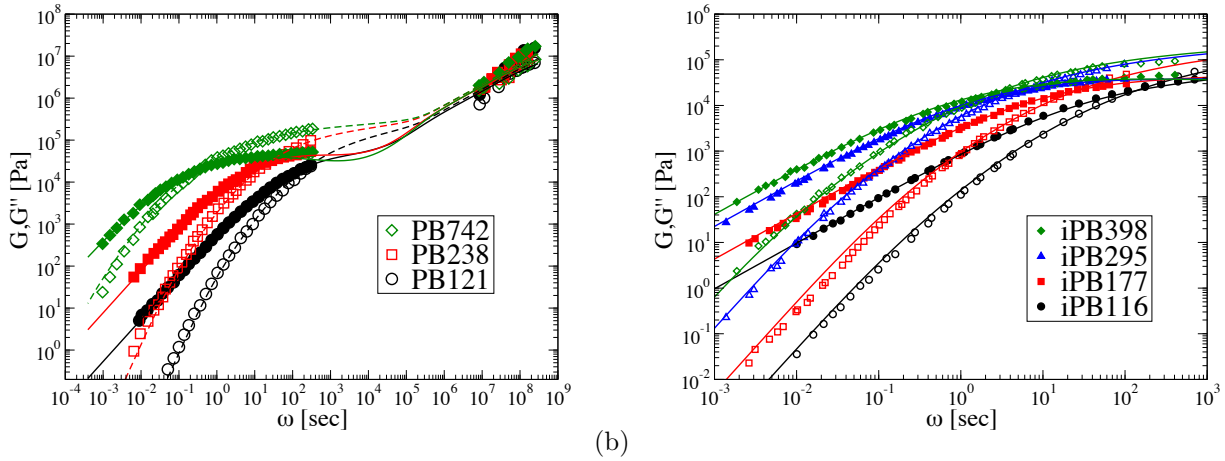

(a) (b)

Figure 3: Extracting tube model parameters and molecular weight distribution from linear rheological measurements, using the BoB model [3]. (a) Linear rheological measurements, augmented with quartz resonator measurements at high frequency by Liu *et al.* [9] at 120°C, using the known MWD to extract M_e. (b) Linear rheological measurements at 140°C by Acierno *et al.* [1] to extract τ_e and confirm the validity of the generalized exponential MWD.

First we compute $\rho_K = 5.3 \times 10^8 \mu\text{m}^{-3}$ from the melt density (Eq.49). For rheological parameters, recent measurements by Liu *et al.*[9] using a quartz resonator have provided the necessary high-frequency LVE, along with full GPC. We use these measurements to determine M_e for iPB before modelling the materials from Acierno *et al.* [1]. BoB fitting using the MWD from GPC is shown in Fig.3(a) for three samples (labels refer to the weight average molecular weight, M_w, in kg/mol). The fit yields $M_e = 9.5$kg mol^{-1}, hence $G_N = 2.6 \times 10^5$Pa (Eq. 50) and $N_e = 9$, and the samples have τ_e values of 2.77, 2.77 and 1.85 μs, respectively, due to the variation in the activation energy.

Having determined M_e, we turn our attention to the LVE data of Acierno *et al.* [1], for which only the weight and number average molecular weights, M_w and M_n, are available (not the full GPC curve). Hence we model the MWD

	Measured quantities			Generalized exponential			Relaxation times (140°C)	
Name	M_w kg/mol	PDI	E_a kJ/mol	M_0 kg/mol	a	b	τ_e (BoB) μs	τ_e (RDP) μs
iPB116	116	3.1	62.5	0.07063	3.0	0.31748	8.6	3.9
iPB177	177	3.3	51.4	9.120	2.0	0.504	8.6	3.5
iPB295	295	4.6	52.7	58.126	1.5	0.6126	8.6	3.3
iPB398	398	3.8	43.1	10.13	2.0	0.4 438	5.73	2.3

Table 2: Sample-dependent quantities and model parameters for the iPB samples from Acierno *et al.*[1]. Measured quantities are reported by Acierno *et al.*. The generalized exponential parameters characterise the MWD, via equation 54 and the relaxation times are fitted to linear rheological data.

Parameter	**Value**	**Method**
Material Parameters		
ρ_K	$5.3\times10^8\mu\text{m}^{-3}$	Literature data and Eq. 49
G_c	0.063μm/sec	Literature value at 103°C [12]
Rheological Parameters		
M_e	9.5 kg mol^{-1}	BoB fit to linear rheology
N_e	9	Eq.51
τ_e (iPB116)	23.4μs ($T = 103$°C)	Rolie-Double-Poly fit to linear rheology
τ_e (iPB177)	15.3μs ($T = 103$°C)	Rolie-Double-Poly fit to linear rheology
τ_e (iPB295)	14.9μs ($T = 103$°C)	Rolie-Double-Poly fit to linear rheology
τ_e (iPB398)	7.9μs ($T = 103$°C)	Rolie-Double-Poly fit to linear rheology
Quiescent Nucleation Parameters		
τ_0	0.31 μs	Projected from τ_e (Eq.53)
N_0 (iPB116)	1.3×10^{-12} μm^{-3}	Fitted to quiescent crystallisation
N_0 (iPB177)	8.3×10^{-12} μm^{-3}	Fitted to quiescent crystallisation
N_0 (iPB295)	12×10^{-12} μm^{-3}	Fitted to quiescent crystallisation
N_0 (iPB398)	37×10^{-12} μm^{-3}	Fitted to quiescent crystallisation
Smooth-polySTRAND model		
μ_S	1.1	Fitted to low shear rate FIC data for iPB116 only
ϵ_B	0.1466	Fitted to low shear rate FIC data for iPB116 only
FIC Parameters		
Γ	1.3	Fitted to low shear rate FIC data for iPB116 only
κ_0	0.1	Obtained from iPP comparison above
Q_{s0}	30.0	Obtained from iPP comparison above

Table 3: Model parameters used to capture the experimentally measured flow-induced turbidity half time, $t_{1/2}$, in iPB [1] using the smooth-polySTRAND model corresponding to results shown in Fig.2(b).

via the generalized exponential distribution

$$W(M) = W_0 \frac{b}{M_0 \Gamma(a/b)} \left(\frac{M}{M_0}\right)^{a-1} \exp\left[-\left(\frac{M}{M_0}\right)^b\right], \tag{54}$$

where Γ is the gamma function and a, b and M_0 are parameters. We constrain b and M_0 to be consistent with the measured M_w and M_n. This leaves a and τ_e to be fitted, for each sample, from the LVE data (Fig.3(b), Table 2). We find that the zero-shear viscosity determines τ_e, while the terminal region of G' is sensitive to a. Having used BoB to ensure we have appropriate M_e and MWDs, we next consider RDP parameters. We fitted τ_e in the linear RDP model to the LVE data for each sample, obtaining a very similar quality of fit to the BoB model (variation in τ_e is shown in Table 2). The τ_e values obtained for the BoB and RDP models differ slightly due to small differences in how the tube model physics is implemented in these two models.

Next we consider the quiescent crystallisation. Fig.2(b) shows experimental crystallisation data of Acierno *et al.* [1], which we can also capture using the smooth-polySTRAND. In Ref.[1] the turbidity half-time, $t_{1/2}$, is measured after quenching to 103°C and occurs when the crystal fraction reaches a fixed value, assumed to be $\phi_c = 10\%$, although our overall conclusions are insensitive to the precise value of this choice. Crystal evolution is computed using the Schneider rate equations [11], which requires knowledge of the crystal growth rate, $G = 0.063\mu$m sec^{-1} for iPB at 103°C [12]. Even quiescently $t_{1/2}$ is dependent on the sample MWD. We attribute this effect to heterogeneous nucleation. By assuming quiescent homogeneous nucleation is negligible, the quiescent $t_{1/2}$ determines the instantaneous nucleation

density, denoted N_0, and gives values of $1.3, 8.3, 12$ and $37 \times 10^{-12}\mu\text{m}^{-3}$ for iPB116, 177, 295 and 398, respectively. The monomer attachment time is $\tau_0 = \tau_K = 0.31\mu$s (Eq.53).

Turbidity is also reported at several shear rates between 0 and 10 s^{-1}; a constant rate shear is applied for shear time t_s, so that $\dot{\gamma}t_s = 60$. In all cases $t_{1/2} \gg t_s$. This shear pulse creates $\dot{N}_{\dot{\gamma}}t_s$ extra nuclei, where $\dot{N}_{\dot{\gamma}}$ is the steady-state FIN rate computed from the smooth-polySTRAND model (we took $Q_{S0} = 30$ and $\kappa_0 = 0.1$ from the iPP comparison above). Thus, to compute the flow-induced $t_{1/2}$ we assume that post-shear nucleation is negligible, and combine $\dot{N}_{\dot{\gamma}}t_s$ and N_0 in the Schneider rate equations. We fitted the remaining parameters, Γ, ΔF_q^* and n^* (via ϵ_B and μ_S), to the FIC data for the lowest molecular weight *only* (iPB166), giving 1.3, $68k_BT$ and 540, respectively; thus the only parameters fitted to FIC data, ϵ_B, μ_S and Γ, are independent of MWD and so require measurements of only one molecular weight sample to predict the remaining materials. Model parameters are summarised in Table 3.

References

[1] S. Acierno *et al.* Effect of molecular weight on the flow-induced crystallization of isotactic poly(1-butene). *Rheologica Acta*, 42(3):243–250, 2003.

[2] V. A. H. Boudara *et al.* Nonlinear rheology of polydisperse blends of entangled linear polymers: Rolie-double-poly models. *Journal of Rheology*, 63(1):71–91, 2019.

[3] C. Das, N. J. Inkson, D. J. Read, M. A. Kelmanson, and T. C. B. McLeish. Computational linear rheology of general branch-on-branch polymers. *J. Rheol.*, 50:207–235, 2006.

[4] R. S. Graham and P. D. Olmsted. Coarse-grained simulations of flow-induced nucleation in semicrystalline polymers. *Phys Rev Lett*, 103(11):115702, 2009.

[5] R. S. Graham and P. D. Olmsted. Kinetic Monte Carlo simulations of flow-induced nucleation in polymer melts. *Faraday Discuss*, 144:71–92, 2010.

[6] M. J. Hamer, J. A. D. Wattis, and R. S. Graham. A method to project the rate kinetics of high dimensional barrier crossing problems onto a tractable 1D system. *Soft Matter*, 8(44):11396–11408, 2012.

[7] K. Jolley and R. S. Graham. A fast algorithm for simulating flow-induced nucleation in polymers. *J Chem Phys*, 134(16):164901, 2011.

[8] K. Jolley and R. S. Graham. Flow-induced nucleation in polymer melts: a study of the GO model for pure and bimodal blends, under shear and extensional flow. *Rheol.Acta*, 52(3):271, 2013.

[9] C. Liu, P. Liu, Q. Chen, B. Du, and Z. Wang. Entanglement relaxation of poly(1-butene) and its copolymer with ethylene detected in conventional shear rheometer and quartz resonator. *Journal of Rheology*, 63(1):167–177, 2019.

[10] R. Pantani *et al.* Shear-induced nucleation and growth in isotactic polypropylene. *Macromolecules*, 43(21):9030–9038, 2010.

[11] W. Schneider, A. Köppl, and J. Berger. Non-isothermal crystallization. Crystallization of polymers. *Int. Polym. Proc. II*, 3:151, 1988.

[12] M. Yamashita and S. Ueno. Direct melt crystal growth of isotactic polybutene-1 trigonal phase. *Crystal Research and Technology*, 42(12):1222–1227, 2019/11/06 2007.